Advanced Composite Materials
Publication details, including instructions for authors and subscription information:
http://www.tandfonline.com/loi/tacm20

On the effects of loading velocity in T-peeling and lap-shearing strengths of FRP

Yukinobu Uchikawa [a], Masaaki Itabashi [b] & Kozo Kawata [c]

[a] Department of Materials Science and Technology, Faculty of Industrial Science and Technology, Science University of Tokyo, 2641, Yamazaki, Noda, Chiba 278, Japan

[b] Department of Materials Science and Technology, Faculty of Industrial Science and Technology, Science University of Tokyo, 2641, Yamazaki, Noda, Chiba 278, Japan

[c] Department of Materials Science and Technology, Faculty of Industrial Science and Technology, Science University of Tokyo, 2641, Yamazaki, Noda, Chiba 278, Japan

Version of record first published: 02 Apr 2012.

To cite this article: Yukinobu Uchikawa , Masaaki Itabashi & Kozo Kawata (1997): On the effects of loading velocity in T-peeling and lap-shearing strengths of FRP, Advanced Composite Materials, 6:4, 279-297

To link to this article: http://dx.doi.org/10.1163/156855197X00148

Adv. Composite Mater., Vol. 6, No. 4, pp. 279–297 (1997)

On the effects of loading velocity in T-peeling and lap-shearing strengths of FRP

YUKINOBU UCHIKAWA, MASAAKI ITABASHI and KOZO KAWATA

Department of Materials Science and Technology, Faculty of Industrial Science and Technology, Science University of Tokyo, 2641, Yamazaki, Noda, Chiba 278, Japan

Received 12 July 1996; accepted 24 October 1996

Abstract—Mechanical properties in T-peeling and lap-shearing of FRP under dynamic load obtained by using the one-bar method are reported. Comparing these with mechanical properties under quasi-static load, positive velocity dependence is clarified in T-peeling strength and lap-shearing strength *vs.* loading velocity relations. The effects of fiber orientation (reinforcement combination) and of the nature of the fiber itself on the strengths of specimens are also clarified.

Keywords: Dynamic T-peeling; dynamic lap-shearing; surface energy; velocity dependence; reinforcement combination.

1. INTRODUCTION

FRP is a very important material for light weight structures in fields such as the automobile and aerospace industries. Recently, demands for the mechanical properties of such structures in dynamic load condition have increased remarkably. Although some data in the research field of high velocity deformation, related to crashworthiness, has already been obtained [1, 2], the studies have mainly concentrated on the tension of general FRP or one dimensionally reinforced plastics. Studies on properties of T-peeling and lap-shearing under dynamic load have not been performed at all. Such advanced characterization should be considered for designing highly and largely integrated structures for vehicles.

In the present article, the tested materials are 2- or 4-ply GFRP, CFRP and KFRP. Reinforcements are both of plain woven cloth (roving cloth) and unidirectionally aligned fibers. Additionally, GFRP reinforced by chopped strand mat is included. The peeling and shearing tests on them are carried out systematically. In such evaluation, maximum load is taken as a representative value of the specimens.

2. EXPERIMENTAL

2.1. Specimen constituents

Specimen constituents are as follows:

GFRP roving cloth

Matrix (Unsaturated polyester Rigolac 158BQT).

Reinforcing fiber (E-glass R-600; Nominal diameter of mono filament: 10 μm; Convergent number of mono filament in strand: 6000).

Reinforcing layer (Product number: WR570B-100; Organization: plain weave, warp 6/25 mm, filling 5.8/25 mm; Weight per unit area: 570 g/m^2).

GFRP chopped strand mat

Matrix (Unsaturated polyester Rigolac 158BQT).

Reinforcing fiber (E-glass CM-450; Nominal diameter of mono filament: 10 μm; Convergent number of mono filament in strand: 400).

Reinforcing layer (Product number: MC450C S-type; Length of strand: 50 mm; Binder: polyester binder; Weight per unit area: 450 g/m^2).

CFRP roving cloth

Matrix (Epoxy resin ACR R97 and hardener ACR H4510).

Reinforcing fiber (Torayca T-300; Nominal diameter of mono filament: 8 μm; Convergent number of mono filament in strand: 6000).

Reinforcing layer (Product number: CO-6644B; Organization: plain weave, warp 10/25 mm, filling 10/25 mm; Weight per unit area: 317 g/m^2).

KFRP roving cloth

Matrix (Epoxy resin ACR R97 and hardener ACR H4510).

Reinforcing fiber (Kevlar-49, Nominal diameter of mono filament: 11.9 μm; Convergent number of mono filament in strand: 7000).

Reinforcing layer (Product number: K-1050; Organization: plain gauze, warp 7/25 mm, filling 7/25 mm; Weight per unit area: 357 g/m^2).

2.1.1. T-peeling test specimen. The size of T-peeling specimens is shown in Fig. 1. The peeling specimens are fabricated by the following process. Firstly, two L-shaped reinforced laminates are made by hand lay-up. Secondly, the laminates are adhered in T-shape by the same matrix resin of the plates. Lastly, the T-shaped assembly is cut into pieces of a required width, 25 mm. The combinations of reinforced laminates are R/R, R/M and M/M for GFRP, and R/R for CFRP and KFRP, where R and M mean roving cloth and chopped strand mat respectively. The roving cloth is set so as to the directions of the specimen of 0° and 90° to the loading direction are reinforced.

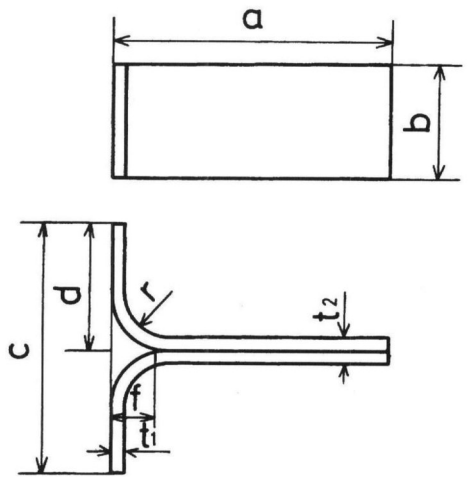

Material	GFRP			CFRP	KFRP
	R/R	R/M	M/M	R/R	R/R
a	40.9	43.9	40.6	41.6	44.8
b	25.0	24.6	25.2	24.9	24.9
c	43.8	45.0	44.9	42.5	46.6
d	21.9	22.5	22.5	21.3	23.3
f	6.0	5.5	6.5	5.0	5.3
t_1	1.2	1.2	1.5	1.3	1.3
t_2	2.3	2.5	2.6	2.6	2.0
r	5.0	5.8	6.0	6.0	6.0

Unit : mm

Figure 1. T-peeling specimen configuration and dimensions.

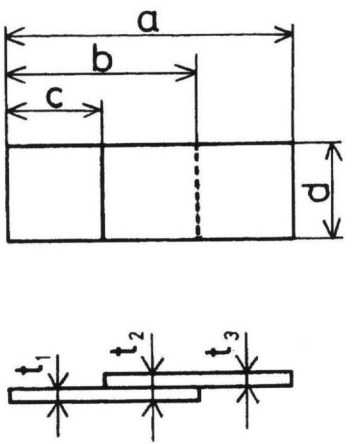

Material	GFRP		
	R/R	R/M	M/M
a	60.7	59.5	61.2
b	40.9	38.7	40.4
c	19.8	20.8	20.8
d	11.1	11.9	11.5
t_1	1.7	1.7	2.0
t_2	4.0	2.8	5.1
t_3	2.3	1.1	3.1

Unit: mm

Figure 2. Lap-shearing specimen configurations and dimensions (for roving cloth and chopped strand mat).

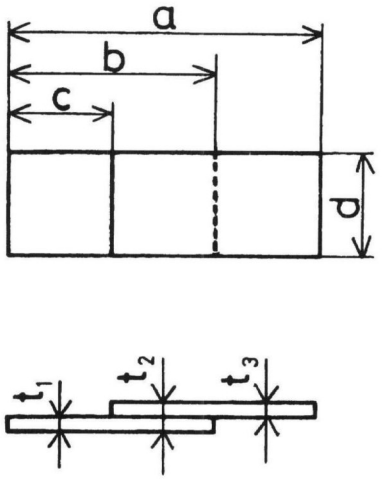

Material	GFRP		
	R／0°／0°／R	R／0°／90°／R	R／90°／90°／R
a	60. 9	59. 3	59. 7
b	40. 5	39. 8	36. 0
c	20. 4	19. 5	23. 8
d	12. 0	12. 4	12. 2
t_1	1. 7	1. 7	1. 9
t_2	3. 0	3. 9	3. 7
t_3	1. 3	2. 2	1. 8

Unit：mm

Figure 3. Lap-shearing specimen configurations and dimensions (for unidirectional reinforcement).

2.1.2. Lap-shearing test specimen. The size of lap-shearing specimens (GFRP) is shown in Figs 2 and 3. Shearing specimens are fabricated by the following process. Firstly, two laminates are made by hand lay-up. Secondly, the laminates are adhered with a required lap length, 20 mm. Lastly, the lapped assembly is cut into pieces of a required width, 12 mm. In Fig. 2, the combinations of laminates are R/R, R/M and M/M for GFRP. To evaluate the effect of unidirectional reinforcement at the surface to be adhered, an extra series of lap-shearing tests were also conducted with the specimen shown in Fig. 3. Their reinforcements are roving cloth/unidirectional/unidirectional/roving cloth. For the unidirectional layers, 0° means the direction of load and 90° means the direction perpendicular to the direction of load. The outer two roving cloth laminates of the extra series of the lap-shearing specimens are just backup ones especially for 90° unidirectional laminates.

2.2. *Principle and practical method for characterization of load–displacement relation in dynamic T-peeling and lap-shearing*

Firstly, the one-bar method [3] of block-to-bar type developed for dynamic tensile testing of solids should be explained briefly. This method has been established as a precise and accurate experimental technique for mechanical characterization in high strain rate tension. In the present series of experiments, a horizontal high velocity tensile loading machine of a slingshot type (Fig. 4) and dynamic tensile load–displacement detection system (Fig. 5) are used. The former was designed to afford an impact force of a hammer (carbon steel, 50 kg) to the specimen via an impact block (Cr–Mo steel, 0.75 kg), which moves on two horizontal parallel rails. As shown in Fig. 6, two aluminum alloy plates with two holes are adhered on loading ends of the specimen by an epoxy adhesive. One plate is attached to the impact block with two screws, and the other plate to an output bar (304 stainless steel, diameter: 10 mm) via a jig of steel. When we roll up rubber ropes on two drums by a worm gear and release the hammer by pulling out a stopper, the hammer is accelerated by the elasticity of the rubber ropes.

When the impact block is given impact by the accelerated hammer, the specimen is deformed dynamically. The velocity of the impact block is 9–11 m/s. The dynamic stress occuring in the specimen is transmitted into the plate as a stress wave. The propagating stress wave is detected by four semiconductor strain gages (Kyowa KSP-2-120-E3, gage length: 2 mm, gage factor: 120) at a gage station on the output bar, located 50 mm from the jig end. The strain gage signal $\varepsilon_g(t)$ corresponds the load–time relation of the specimen. Velocity of the impact block $V(t)$ is monitored by an electrooptical displacement transducer (Zimmer model 100D/II) and a differentiator (Zimmer model 131C). Both signals, $\varepsilon_g(t)$ and $V(t)$ are stored in two synchronized digital memories (Kawasaki Electronica TMR-100, sampling frequency: 1 MHz, capacity: 4 kwords) respectively and are converted to load–time and displacement–time relations by a personal computer (NEC PC-8801 mk II). Then, eliminating time from the two relations, a load–displacement curve is obtained. Details of the data reduction may be found in [4].

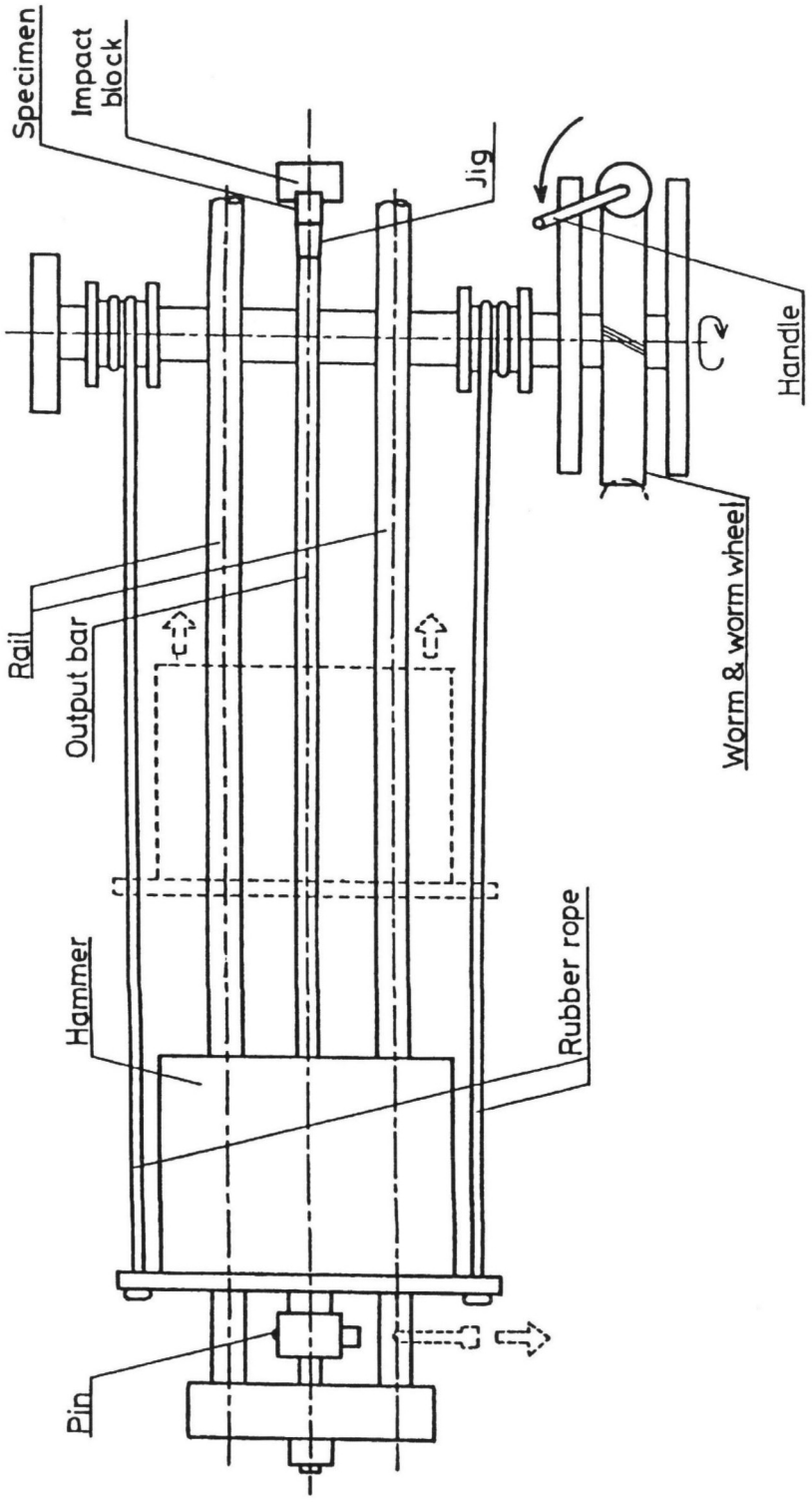

Figure 4. Dynamic tensile loading machine of a slingshot type.

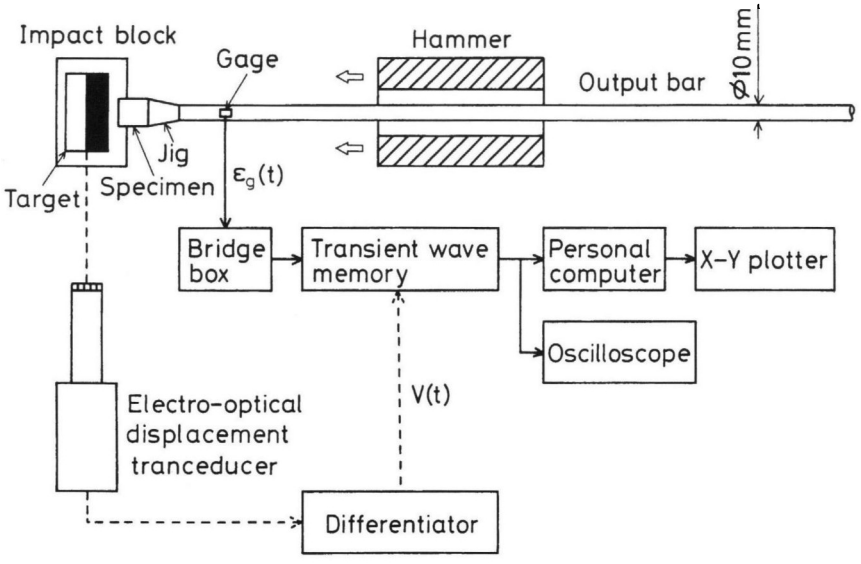

Figure 5. Block diagram of dynamic tensile load–displacement detection system.

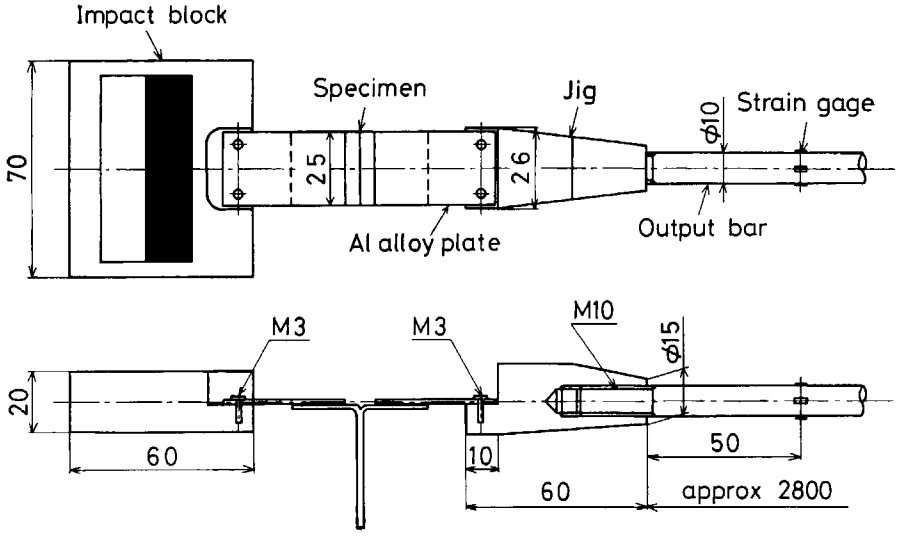

Figure 6. Detail of specimen mounting on dynamic tensile loading machine (for T-peeling specimen).

2.3. Quasi-static T-peeling and lap-shearing tests

In order to evaluate the quasi-static mechanical properties, quasi-static tests are also performed at the loading velocity of 5.0 mm/min (equivalent to 0.000083 m/s) with a universal material testing machine (Shimadzu Autograph AGS-500A, capacity: 4.9 kN) and the same design of the specimens.

3. RESULTS AND DISCUSSION

3.1. Results of T-peeling tests

3.1.1. T-peeling load–displacement relations. Typical T-peeling load–displacement curves under the quasi-static and dynamic load for GFRP(R/M) are shown in Fig. 7. For the quasi-static curve, the load increases quite sharply and decreases gradually with progress of peeling. On the other hand, for the dynamic curve, the load shows the second peak higher than both the quasi-static peak and the dynamic first one. From the standpoint of practical evaluation, the present authors take the maximum load value as the peeling strength.

3.1.2. Fracture appearance. Fractured surfaces are shown in Fig. 8. As shown in (b) and (c), fracture seems occur in the chopped strand mat layer. In (a), small parts of fibers adhering to another piece are seen.

3.1.3. Maximum peeling load vs. *velocity relation.* The relations between the maximum load and loading velocity on the peeling test are shown in Figs 9a, b. Figure 9a indicates the effect of the combination of reinforcement for GFRP, and Fig. 9b shows the effect of fiber itself for the reinforcement R/R.

In Fig. 9a, the maximum peeling load increases with increasing loading velocity for GFRP regardless of the reinforcement combination and it shows positive dependence. The maximum peeling loads vary with the reinforcement combinations for GFRP, such as R/R, R/M and M/M. The values for R/M and M/M are higher than for R/R

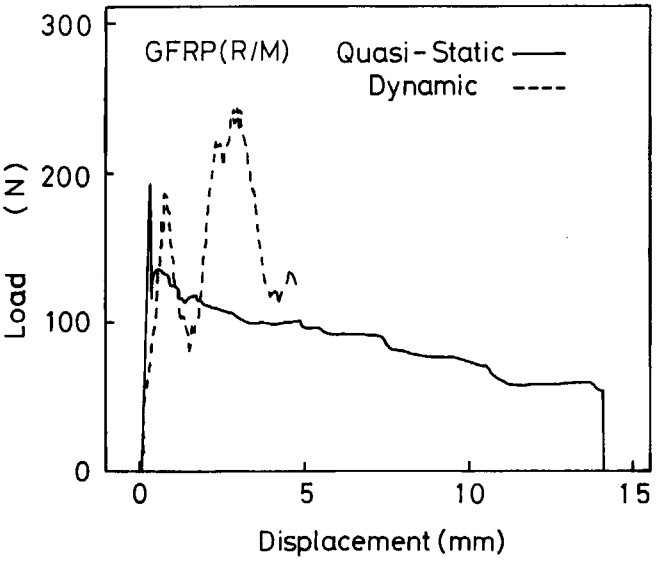

Figure 7. Typical T-peeling load–displacement curves for GFRP(R/M) specimen (quasi-static loading velocity: 5.0 mm/min; dynamic loading velocity: 9.2 m/s).

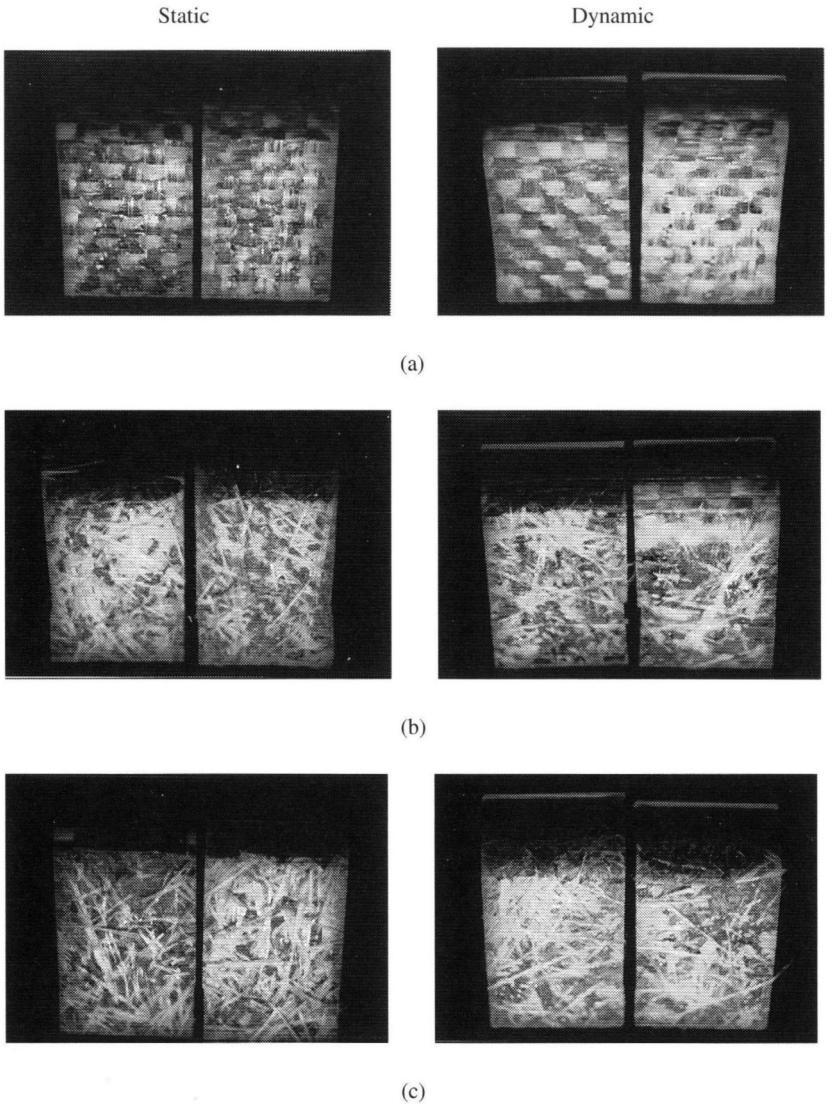

Figure 8. Fractured surface of T-peeling specimens: (a) GFRP(R/R); (b) GFRP(R/M); (c) GFRP(M/M).

under both quasi-static and dynamic peeling. So, it can be said that chopped strand mat is effective in increasing T-peeling load. It is considered that for chopped strand mat with random fiber orientation, an anchor effect is expected, and at the same time, micro-fractures are not unidirectional but distributed.

In Fig. 9b, the effect of the different types of reinforcing fiber, for the reinforcement R/R, is observed. That is, their peeling loads are in the order of KFRP > CFRP > KFRP for the reinforcement R/R. For CFRP, two groups are observed in dynamic tension. For the lower group, it seems that some vacancies, such as air holes, exist at the peeling edge, as shown in Fig. 10.

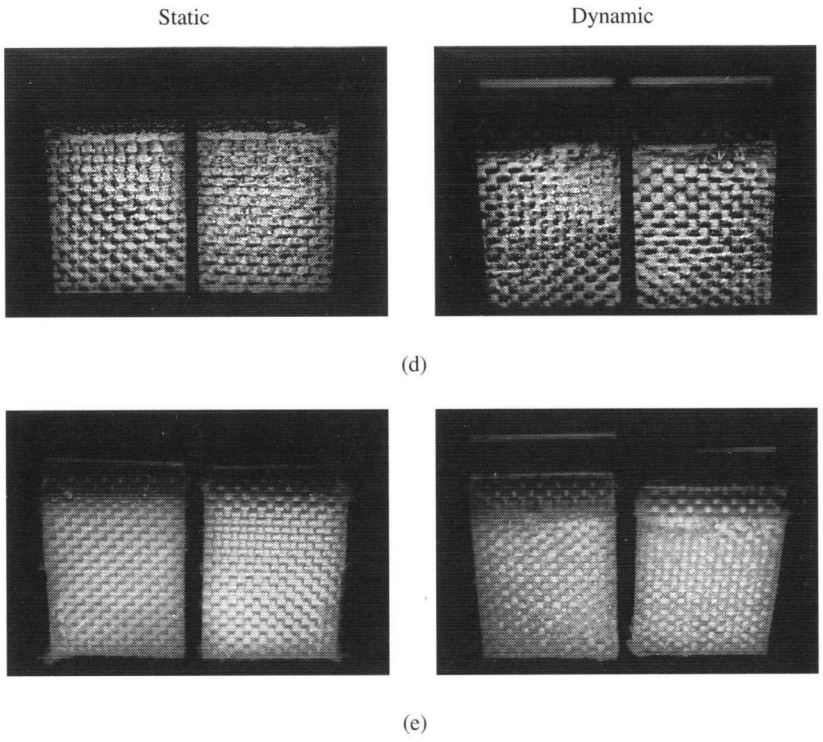

Figure 8. (Continued). (d) CFRP(R/R); (e) KFRP(R/R).

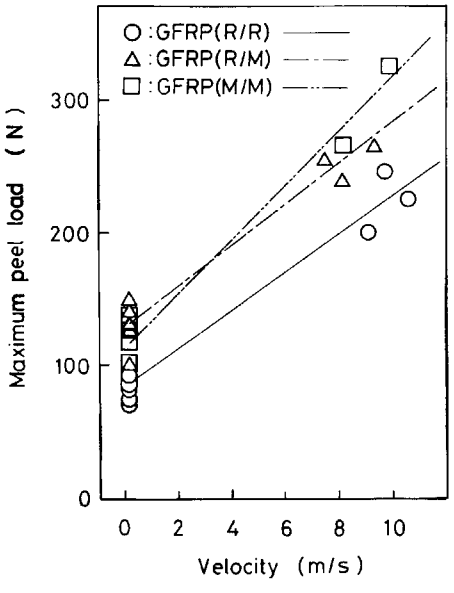

Figure 9a. Experimental results of maximum peeling load–velocity relations for GFRP(R/R), GFRP (R/M) and GFRP(M/M).

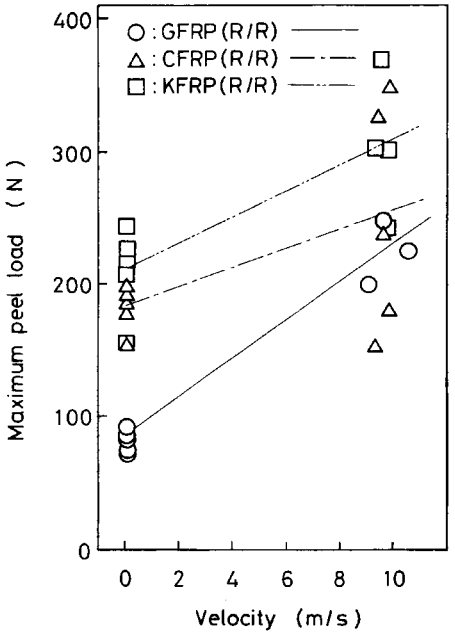

Figure 9b. Experimental results of maximum peeling load–velocity relations for GFRP(R/R), CFRP(R/R) and KFRP(R/R).

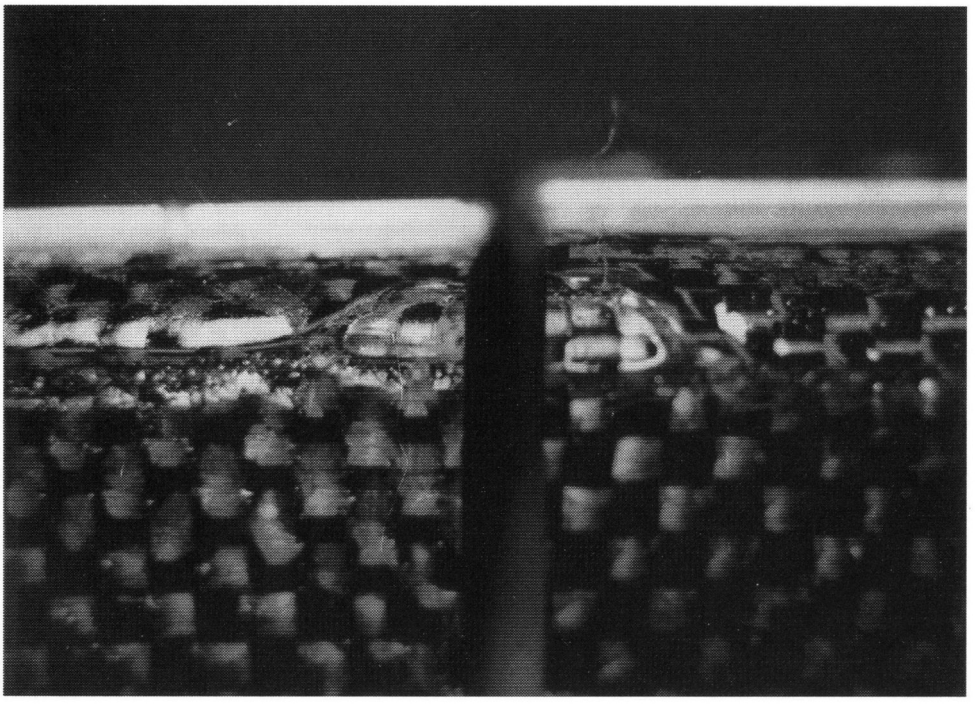

Figure 10. Air hole in CFRP specimen.

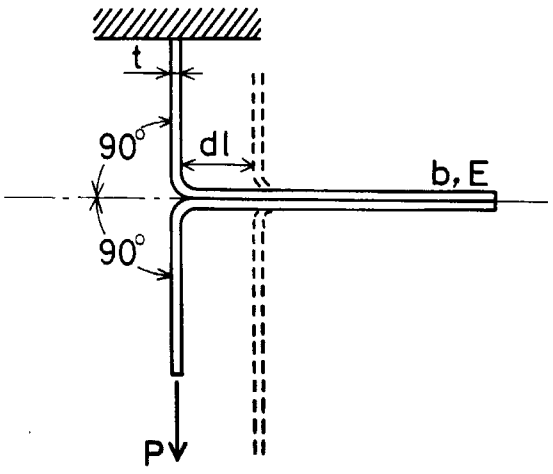

Figure 11. Surface energy of T-shaped adhesive peeling.

3.1.4. Peeling surface energy vs. *velocity relation.* On the peeling surface energy of T-shaped adhesive peeling, a theoretical equation is derived by Kawata and Fukuda [5] assuming rather low rigidity of materials. By this analysis,

$$\gamma_1 = \frac{P}{b}, \tag{1}$$

where γ_1, P and b are the peeling surface energy, peeling breaking load and width of specimen, respectively. γ_1 is obtained using (1) tentatively, although the rigidity of FRP is not stated to be 'rather low'. The relation between the peeling surface energy and velocity are shown in Figs 12a, b. If we take P at the maximum peeling value, the peeling surface energy shows positive velocity dependence similar to the maximum peeling load.

3.2. Results of lap-shearing tests

3.2.1. Lap-shearing load–displacement relations. Typical shearing load–displacement curves under quasi-static and dynamic tensile load obtained for GFRP(R/M) and GFRP(R/0°/0°/R) are shown in Figs 13 and 14, respectively. In both cases, the shearing load increases sharply and decreases suddenly with the beginning of catastrophic shear fracture.

3.2.2. Fracture appearance. Fractured surface are shown in Figs 15 and 16. In (b) and (c) fracture in the 90° layers is observed.

3.2.3. Maximum shearing load vs. *velocity relation.* The relations between maximum shearing load and velocity in the lap-shearing tests are shown in Fig. 17 for the combination of R/R, R/M and M/M and in Fig. 18 for the combination of R/0°/0°/R, R/0°/90°/R, R/90°/90°/R.

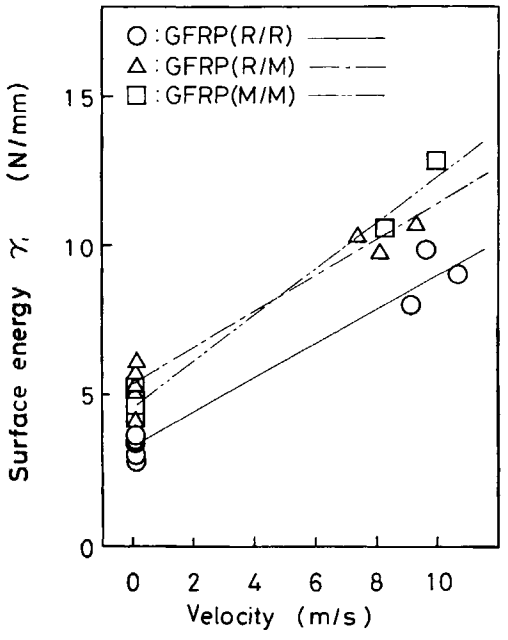

Figure 12a. Experimental results of surface energy–velocity relations for GFRP(R/R), GFRP(R/M) and GFRP(M/M).

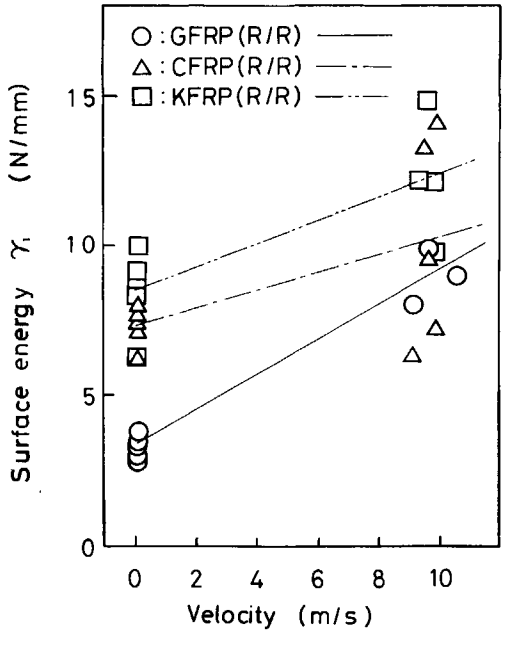

Figure 12b. Experimental results of surface energy–velocity relations for GFRP(R/R), CFRP(R/R) and KFRP(R/R).

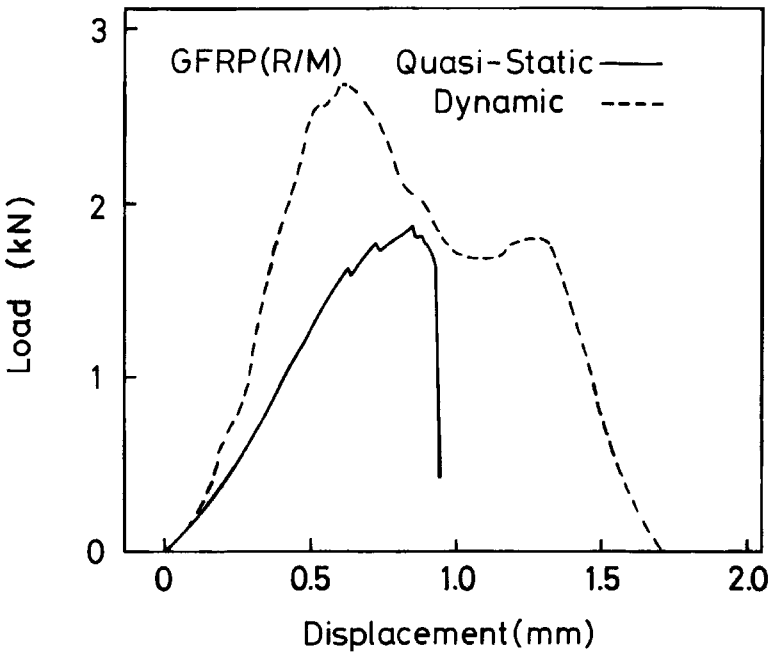

Figure 13. Typical lap-shearing load–displacement curves for GFRP(R/M) specimen (quasi-static loading velocity: 5.0 mm/min; dynamic loading velocity: 8.9 m/s).

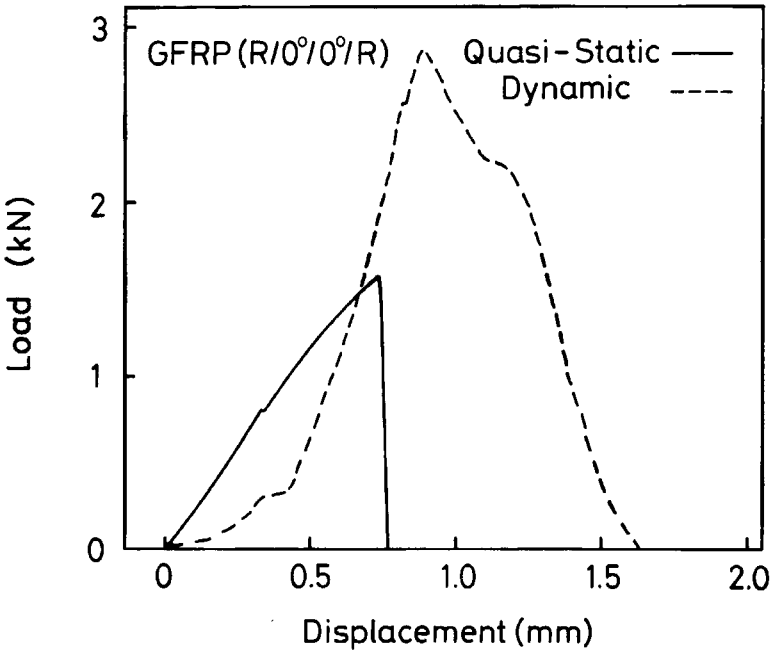

Figure 14. Typical lap-shearing load–displacement curves for GFRP(R/0°/0°/R) specimen (quasi-static loading velocity: 5.0 mm/min; dynamic loading velocity: 8.8 m/s).

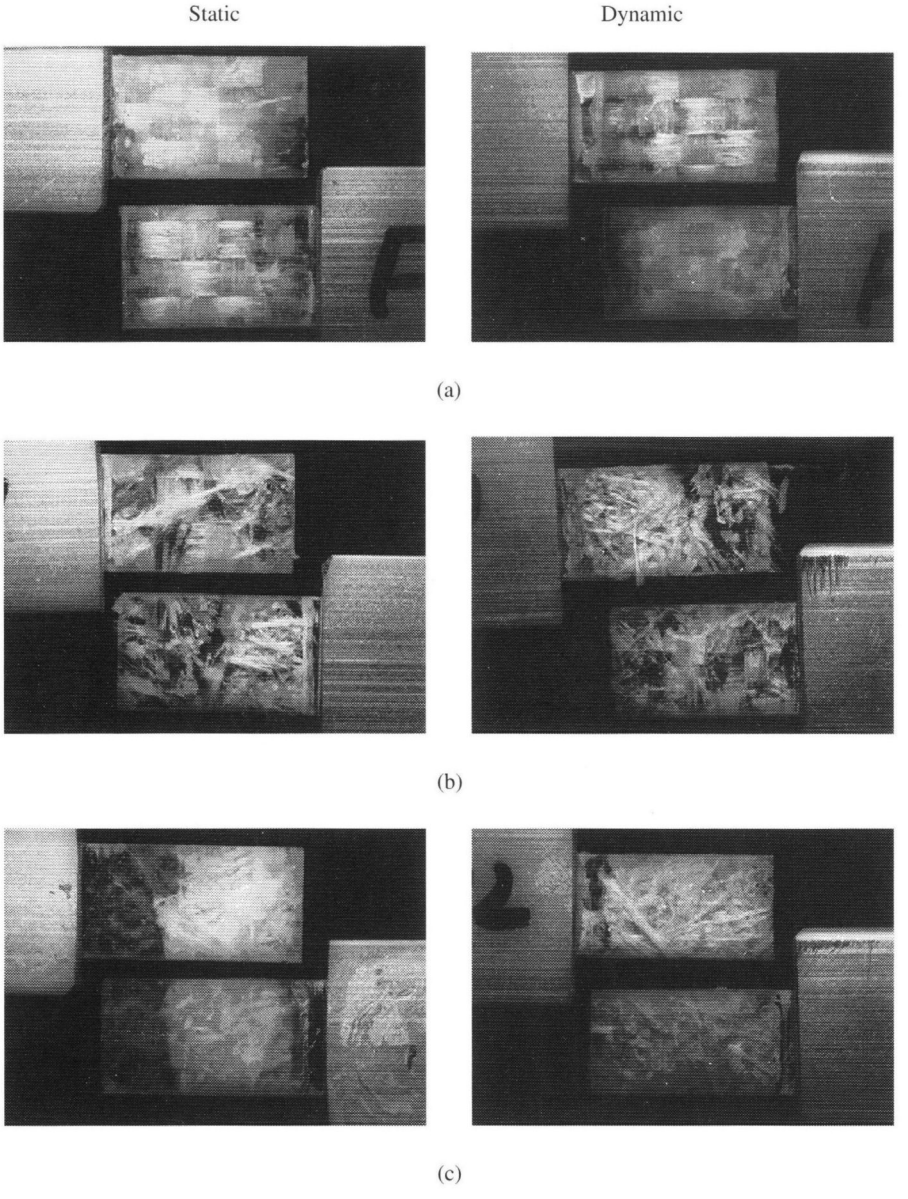

Figure 15. Fractured surface of lap-shearing specimens (for roving cloth and chopped strand mat): (a) GFRP(R/R); (b) GFRP(R/M); (c) GFRP(M/M).

In Fig. 17, the effect of the reinforcement combinations for GFRP is observed, that is, the shearing strengths are in the order of R/M, R/R and M/M under both quasi-static and dynamic load. The scattering range for each of them is relatively wider than that of the maximum peeling load.

Figure 18 shows the relations between the maximum shearing load and velocity of specimens of which adhered faces are reinforced unidirectionally by long fibers. In

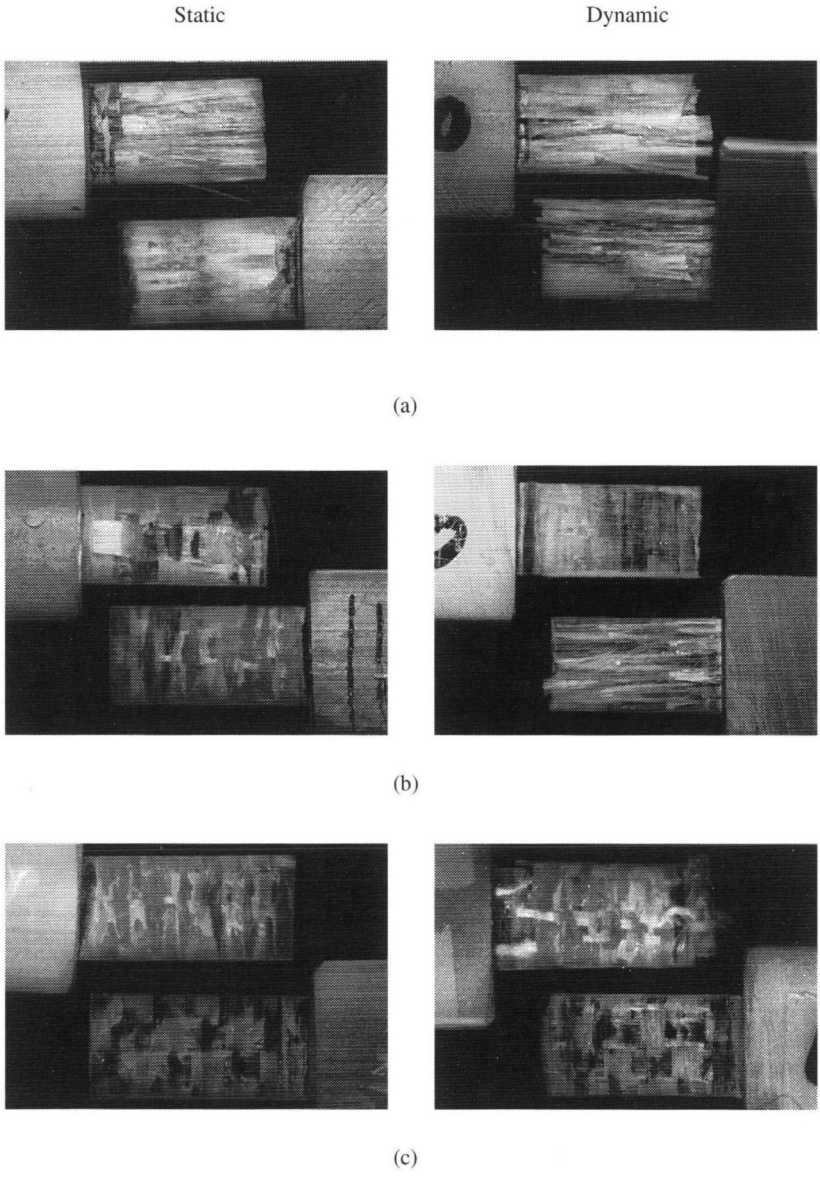

Figure 16. Fractured surface of lap-shearing specimens (for unidirectional reinforcement): (a) GFRP(R/0°/0°/R); (b) GFRP(R/0°/90°/R); (c) GFRP(R/90°/90°/R).

Fig. 18, the maximum shearing loads appear in the order R/0°/0°/R > R/0°/90°/R > R/90°/90°/R for GFRP. In the 90° unidirectional reinforcement layer, the strength for the load is considered to be determined mainly by the matrix resin. On the other hand, in the 0° unidirectional reinforcement layer, the strength for the load is considered to be determined mainly by the fiber. So, the above mentioned order is considered to be reasonable.

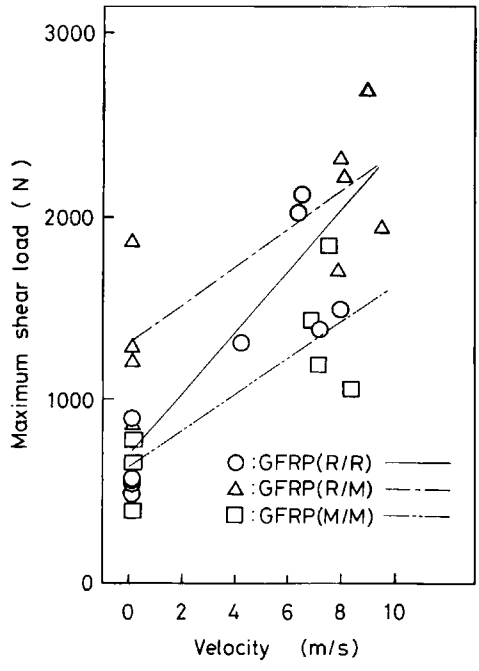

Figure 17. Experimental results of maximum shearing load–velocity relations for GFRP(R/R), GFRP (R/M) and GFRP(M/M).

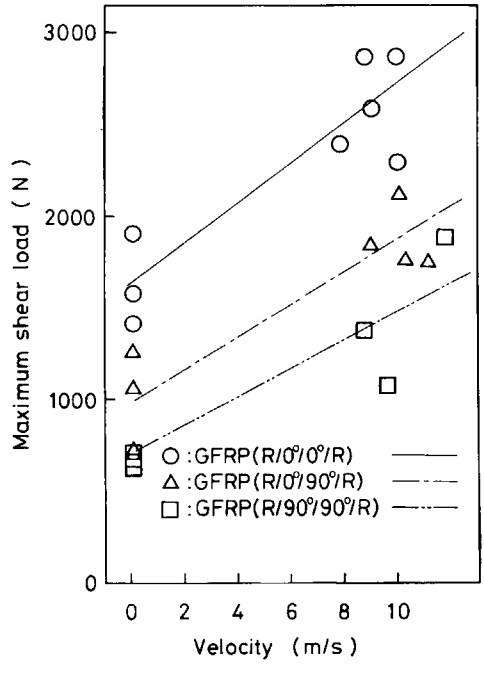

Figure 18. Experimental results of maximum shearing load–velocity relations for GFRP(R/0°/0°/R), GFRP(R/0°/90°/R) and GFRP(R/90°/90°/R).

4. CONCLUSIONS

From the quasi-static and dynamic tests described above for T-peeling of GFRP, CFRP and KFRP and quasi-static and dynamic tests for lap-shearing of GFRP, the following facts have been established.

(1) In T-peeling of FRP, the maximum value of peeling load and corresponding surface energy show positive loading velocity dependence and the values and rate of increase are different according to the type of reinforcing fiber and reinforcement combination.

(2) In T-peeling of GFRP, the use of chopped strand mat tends to be more effective in increasing peeling strength than the use of roving cloth. In the peeling of GFRP, CFRP and KFRP for the R/R reinforcement, the strengths are in the order of KFRP > CFRP > GFRP for both quasi-static and dynamic tests.

(3) In lap-shearing of GFRP, the maximum value of shearing load shows positive loading velocity dependence. The maximum shearing load and its rate of velocity increase depend upon the reinforcement combination.

(4) In quasi-static and dynamic lap-shearing of GFRP, the strengths are in the order of R/M > R/R > M/M and R/M/0°/0°/R > R/0°/90°/R > R/90°/90°/R.

(5) It is interesting that although the effects of fiber orientation for peeling strength and for lap-shearing strength of GFRP do not necessarily perfectly coincide, R/M is a relatively well-balanced combination overall.

Acknowledgements

The authors wish to express their hearty thanks to Professor H. Fukuda for his kind discussions, to DJK Research Center Inc. for supply of suitable FRP specimens, and to Messrs. Masaki Nakajima and Toshiyuki Higuchi for their eager assistance in carrying out the series of experiments.

REFERENCES

1. Kawata, K., Hashimoto, S., Takeda, N. and Chung, H.-L. Dynamic behaviour analysis of composite materials. In: *Composite Materials: Mechanics, Mechanical Properties and Fabrication*, Kawata, K. and Akasaka, T. (Eds). Japan Society for Composite Materials (1981), pp. 2–11.
2. Kawata, K., Hashimoto, S. and Takeda, N. Mechanical behaviour in high velocity tension of composites. In: *Progress in Science and Engineering of Composites*, vol. 1, Hayashi, T., Kawata, K. and Umekawa, S. (Eds). North-Holland, (1982), pp. 829–836.
3. Kawata, K., Hashimoto, S., Kurokawa, K. and Kanayama, N. A new testing method for the characterization of materials in high velocity tension. In: *Mechanical Properties at High Rates of Strain, 1979*, Harding, J. (Ed.). Conference Series No. 47, Institute of Physics, Bristol and London (1979), pp. 71–80.
4. Kawata, K., Chung, H.-L. and Itabashi, M. Dynamic mechanical behavior of HTPB dummy composite propellant. *Adv. Compos. Mater.* **3**, 163–175 (1994).
5. Kawata, K. and Fukuda, H. Analysis of peeling fracture of adhesive. *Trans. JSCM* **1**, 36–39 (1975).